Characterization of Thermospheric Vertical Wind Activity at 225- to 295-km Altitude Using GOCE Data and Validation Against Explorer Missions

Visser, T.; March, G.; Doornbos, E. N.; de Visser, C. C.; Visser, P. N.A.M.

DOI
10.1029/2019JA026568

Publication date
2019

Document Version
Final published version

Published in
Journal of Geophysical Research: Space Physics

Citation (APA)
Visser, T., March, G., Doornbos, E. N., de Visser, C. C., & Visser, P. N. A. M. (2019). Characterization of Thermospheric Vertical Wind Activity at 225- to 295-km Altitude Using GOCE Data and Validation Against Explorer Missions. *Journal of Geophysical Research: Space Physics*, *124*(6), 4852-4869. https://doi.org/10.1029/2019JA026568

JGR Space Physics

RESEARCH ARTICLE
10.1029/2019JA026568

Characterization of Thermospheric Vertical Wind Activity at 225- to 295-km Altitude Using GOCE Data and Validation Against Explorer Missions

T. Visser[1], G. March[1], E. N. Doornbos[1], C. C. de Visser[1], and P. N. A. M. Visser[1]

[1]Faculty of Aerospace Engineering, Delft University of Technology, Delft, The Netherlands

Key Points:
- Vertical wind standard deviations derived from linear accelerations are consistent with those derived from mass spectrometry
- Geomagnetic activity and local time are main drivers of vertical wind activity at high latitudes; local time and season at low latitudes
- The vertical wind standard deviation levels out at 10–50 m/s (5th and 95th percentiles) for AE index levels above 800

Correspondence to:
T. Visser
t.visser-1@tudelft.nl

Citation:
Visser, T., March, G., Doornbos, E. N., de Visser, C. C., & Visser, P. N. A. M. (2019). Characterization of thermospheric vertical wind activity at 225- to 295-km altitude using GOCE data and validation against Explorer missions. *Journal of Geophysical Research: Space Physics*, *124*. https://doi.org/10.1029/2019JA026568

Received 29 JAN 2019
Accepted 21 MAY 2019
Accepted article online 29 MAY 2019

Abstract Recently, the horizontal and vertical cross wind at 225- to 295-km altitude were derived from linear acceleration measurements of the Gravity field and steady-state Ocean Circulation Explorer satellite. The vertical component of these wind data is compared to wind data derived from the mass spectrometers of the Atmosphere Explorer C and E and Dynamics Explorer 2 satellites. From a statistical analysis of the 120-s moving-window standard deviation of the vertical wind ($\sigma(V_z)$), no consistent discrepancy is found between the accelerometer-derived and the mass spectrometer-derived data. The validated Gravity field and steady-state Ocean Circulation Explorer data are then used to investigate the influence of several parameters and indices on the vertical wind activity. To this end, the probability distribution of $\sigma(V_z)$ is plotted after distributing the data over bins of the parameter under investigation. The vertical wind is found to respond strongly to geomagnetic activity at high latitudes, although the response settles around a maximum standard deviation of 50 m/s at an Auroral Electrojet index of 800. The dependence on magnetic local time changes with magnetic latitude, peaking around 4:30 over the polar cap and around 01:30 and 13:30 in the auroral oval. Seasonal effects only become visible at low to middle latitudes, revealing a peak wind variability in both local summer and winter. The vertical wind is not affected by the solar activity level.

1. Introduction

The purpose of this paper is to identify and characterize the drivers of vertical wind activity in the thermosphere at 225- to 295-km altitude, from a dusk-dawn orbit that covers all magnetic latitudes. We do so by introducing, validating, and analyzing a new vertical wind data set derived from linear acceleration data of the Gravity field and steady-state Ocean Circulation Explorer (GOCE) satellite (Floberghagen et al., 2011). The detailed discussion of the vertical wind response to a range of parameters, namely, magnetic latitude, geomagnetic activity, local time, season, and solar activity, may aid atmosphere modelers in their efforts to capture the behavior of the thermosphere.

Vertical wind in the thermosphere is characterized by peaks in the auroral oval and polar cap regions, sometimes exceeding 100 m/s (Innis et al., 1999; Smith & Hernandez, 1995, e.g.). They are concentrated in the midnight-dawn sector in terms of magnetic local time (Innis & Conde, 2002). On top of that, local vertical velocity enhancements have been observed of 10–50 m/s, not limited to the high-latitude regions (Anderson et al., 2012; Larsen & Meriwether, 2012). These enhancements may persist for several hours and have been linked to local time, being predominantly downward during the day and upward around midnight (Smith & Hernandez, 1995; Sipler et al., 1995).

Currently, the primary source of vertical wind measurements in the *F* region is ground-based Fabry-Perot Interferometry (Anderson et al., 2012). These wind measurements are inferred from the Doppler shift in the nighttime emission at specific wavelengths. Downsides of this method include the limited spatial distribution of measurement stations and the requirement of nighttime clear-sky conditions. On top of that, Fabry-Perot Interferometry depends on a choice for a zero Doppler baseline (Anderson et al., 2012; Aruliah & Rees, 1995; Larsen & Meriwether, 2012). It has been suggested by Harding et al. (2017) that, combining all measurements errors, large wind measurements may be up to 100% uncertain. The major secondary source of vertical wind data is in situ mass spectrometry. These data were collected by the Atmosphere Explorer C (AE-C) and E (AE-E) (Spencer et al., 1973) and Dynamics Explorer 2 (DE-2) satellites (Hoffman, 1980). Depending on the orbit, satellites can provide global coverage at arbitrary local times. The AE-C mission was

designed to focus on auroral latitudes, leading to a better understanding of aurora-induced gravity waves (Knutson et al., 1977; Spencer et al., 1976). The AE-E satellite on the other hand had an equatorial orbit. Finally, DE-2 provided global coverage of vertical wind data for the first time, which led to the statistical analysis of Innis and Conde (2002) that we have adopted for this work as well.

The new vertical wind data presented in this paper were obtained from the GOCE linear accelerations, which were used to produce thermospheric horizontal wind and neutral density data (Doornbos, 2016) and to investigate thermospheric wave activity (Garcia et al., 2013; Trinh et al., 2018) in the past. The way of deriving these data is described in detail by Visser et al. (2019). In this paper we closely follow the statistical analysis of Innis and Conde (2002) to compare the accelerometer-derived data from GOCE to the spectrometer-derived data from the three aforementioned missions. First, we calculate the moving-window standard deviation of the vertical wind $\sigma(V_z)$ for all data sets. The GOCE data are validated against the other satellite measurements by comparing the probability distributions of this parameter under specific, fixed conditions. Finally, we take advantage of the size of the new data set to analyze how the vertical wind activity changes with some key parameters and indices. In this process the data are first distributed over bins of a vertical wind driver (such as the Auroral Electrojet (AE) geomagnetic index; Neil Davis & Sugiura, 1966), before calculating the probability distribution of the $\sigma(V_z)$ parameter in each bin. The resulting plot is used to characterize the response of the vertical wind to the driving parameter.

Because of its high data rate (currently interpolated at 0.1 Hz) and continuous 4-year operation (resulting in 1,100 full days of 16 orbits and another 170 days of partial operation), GOCE single-handedly provides 26 times as many thermospheric vertical wind data as the three aforementioned Explorer missions combined. Merely the size of the data set may therefore spark new investigations into this component of thermosphere research. In the results of our analysis, we observe evidence of an upper limit to the vertical wind activity due to geomagnetic storms. The existence, value, and criteria for occurrence of this upper limit can contribute to the understanding of atmospheric damping and the subsequent modeling of these effects in whole atmosphere models. The most prominent vertical wind features are short-lived, local wavelets with amplitudes up to 150 m/s near the auroral oval and over the polar cap. Especially these signals have the potential to support research into the occurrence and origins of gravity waves.

The paper is structured as follows. The data used in this work are presented in section 2, and their distribution over several driving parameters is discussed. Then, in section 3, the data processing is described, as well as the definition of the main plots in this work. The GOCE vertical wind measurements are compared to those from the other satellites in section 4. The results are then discussed in section 5, in which the dependence of vertical wind activity on several parameters is shown. Finally, in section 6, the conclusions of this work are drawn.

2. Data

All data used in this work are taken from satellite missions. The first three, AE-C, AE-E, and DE-2, were dedicated atmospheric research missions, whereas GOCE was initially intended for gravity field and ocean circulation studies only. In this section, we describe the data sets in terms of the required processing steps and their distribution over time, altitude, latitude, and solar and geomagnetic activities.

In Table 1, some key characteristics of the data sets are listed. Although the Atmosphere Explorers had a high apogee, around 4,000 km, no data was gathered by these two missions above 600 km. Instead, the eccentricity of the orbit was meant to allow a deep dip into the atmosphere, which is especially clear for AE-C. The DE-2 orbit was polar, resulting in global coverage, both geographically and in local time. GOCE, on the other hand, was in a near-polar, sun-synchronous orbit, resulting in near-global geographic coverage and dusk-dawn coverage in local time. The offset of the magnetic poles from the Earth's rotation axis does however result in a sufficient variation in magnetic local time to allow a comparison with DE-2 in section 4.

AE-C, AE-E, and DE-2 used mass spectrometers to measure the vertical wind. The Neutral-Atmosphere Temperature Experiment (NATE, on the AE satellites) and the Wind And Temperature Spectrometer (WATS) infer the wind from density measurements. As the density is being measured, a baffle moves past the orifice through which the atmospheric particles enter the measurement chamber. This creates a dip in the density as the baffle blocks the incoming particles from directly entering the chamber. The incoming flow direction is inferred from the baffle position that blocks most of the particles. Combined with the atti-

Table 1
Orbit and Data Set Characteristics of the Four Satellites Used in This Study

Mission	Years of data	Altitude (km)	Inclination (deg)	Instrument	Reference
AE-C	1973–1977	134–4,000	68	NATE[a]	Spencer et al. (1973)
AE-E	1975–1977	248–4,000	19.7	NATE[a]	Spencer et al. (1973)
DE-2	1981–1983	210–1,012	89.99	WATS[b]	Hoffman (1980)
GOCE	2009–2013	225–295	96.7	EGG[c]	Floberghagen et al. (2011)

Note. AE-C and AE-E = Atmosphere Explorers C and E; DE-2 = Dynamics Explorer 2; GOCE = Gravity field and steady-state Ocean Circulation Explorer; NATE = Neutral Atmosphere Temperature Experiment; WATS = Wind And Temperature Spectrometer; EGG = Electrostatic Gravity Gradiometer.
[a] NATE: scanning neutral mass spectrometer. [b] WATS: scanning mass spectrometer. [c] EGG: three orthogonal pairs of three-axis accelerometers.

tude and orbital velocity information, this flow direction results in a wind measurement (Spencer et al., 1976, 1982).

The algorithm to obtain vertical wind from the linear accelerations of a satellite has been extensively described by Visser et al. (2019). In short, the solar radiation pressure and thrust force are modeled and deducted from the measured acceleration. Assuming the remaining signal is aerodynamic, the direction of the incoming flow can be derived by matching an aerodynamic model with the residual acceleration. The incoming flow vector is reduced by the orbital velocity, such that the wind remains. The total (three-dimensional) wind measurements obtained from GOCE are rotated from the satellite body frame (in which they are derived) to the local orbit frame. In this paper, we focus solely on the vertical wind component in this frame. The data set spans 4 years of global and continuous operation at altitudes between 225 and 295 km. It includes quiet and disturbed times (up to Kp 8−), a wide range of solar activity (F10.7 from 68 to 182), but only a limited local time (equator crossings at 06:22–7:52 [descending] and 18:22–19:52 [ascending]). On top of that, the GOCE orbit is tilted a few degrees toward the Sun in the North and away from the Sun in the South, which leads to longer eclipses on the Southern Hemisphere.

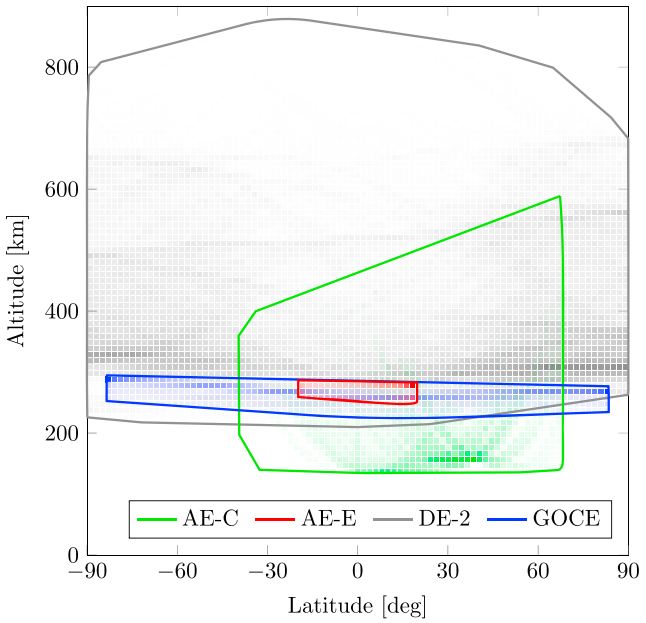

Figure 1. Distribution and convex hull of vertical wind data over latitude and altitude for all four satellites. The opacity indicates the data density as a percentage of the most densely packed bin per satellite. AE-C and AE-E = Atmosphere Explorers C and E; DE-2 = Dynamics Explorer 2; GOCE = Gravity field and steady-state Ocean Circulation Explorer.

To obtain a more comprehensive overview of the data availability, the data density is plotted over latitude and altitude in Figure 1, over Kp and F10.7 in Figure 2, and over magnetic local time and day of year in Figure 3. The intensity of the color indicates the data density compared to the most densely packed bin for that satellite; the solid line indicates the contour of the convex hull of the data set. In Figure 1, we can clearly identify the limitations in latitude and altitude imposed by the orbit geometries. The Atmosphere Explorers are particularly limited in their latitude range by their inclination, while DE-2 and GOCE show a concentration of data at high latitudes. The distributions over Kp index (which is, contrary to the AE-index, available for AE-E) and F10.7 flux in Figure 2 show a clear distinction between the quiet GOCE mission and the active DE-2 mission. The Atmosphere Explorers were, like GOCE, operated during a solar minimum. Finally, the precession of the orbits over a year can be inferred from Figure 3. Most importantly, the GOCE orbit remains mostly fixed in local time throughout the year, thus preventing any cross contamination between local time and seasonal variations. Note that the bulk of GOCE measurements are taken at dawn and dusk; the full range of local times is only available during polar passes. The measurements of AE-C, however, are concentrated along a few lines of local time and day of year. AE-E has only measured vertical wind during the Northern summer period.

The different data sets have different causes and levels of uncertainty. Spencer et al. (1976) analyzed the five main error sources for vertical wind measurements of the NATE instrument on AE-C. They found that the total error will not exceed 5 m/s. This error excludes the uncertainty in

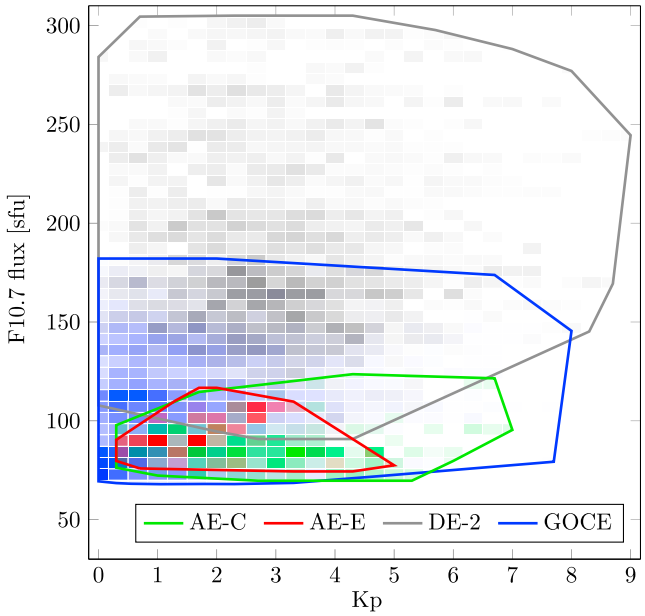

Figure 2. Distribution and convex hull of vertical wind data over Kp index and F10.7 daily observed flux for all four satellites. The opacity indicates the data density as a percentage of the most densely packed bin per satellite. AE-C and AE-E = Atmosphere Explorers C and E; DE-2 = Dynamics Explorer 2; GOCE = Gravity field and steady-state Ocean Circulation Explorer.

the spacecraft attitude measurement, which causes an estimated uncertainty of 20–30 m/s in the average vertical wind for DE-2 (Spencer et al., 1982). Assuming that the Atmosphere Explorers and DE-2 have similar characteristics, we conclude that the uncertainty in the mass spectrometer data is characterized by a maximum 30 m/s bias and maximum 5 m/s random error. The average wind level is also the largest uncertainty in the GOCE data. Judging from the sensitivity analysis of Visser et al. (2019), a bias of at least 3 m/s is possible. To arrive at the current GOCE vertical wind data, however, several parameters were estimated in

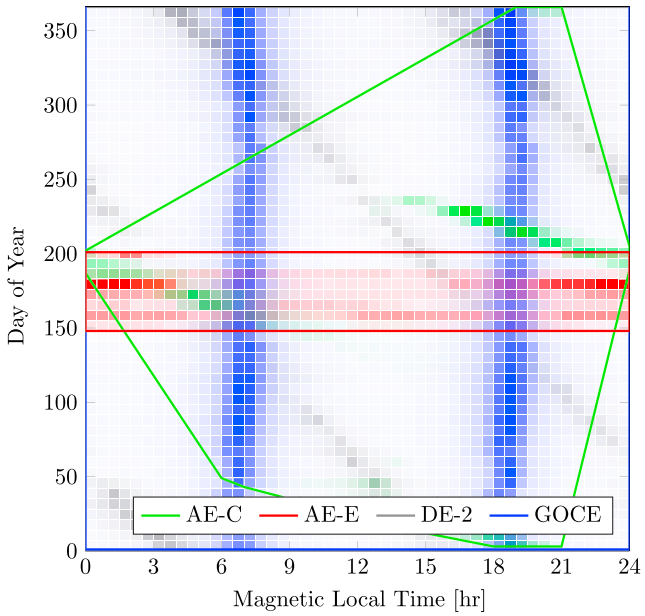

Figure 3. Distribution and convex hull of vertical wind data over magnetic local time and day of year for all four satellites. The opacity indicates the data density as a percentage of the most densely packed bin per satellite. AE-C and AE-E = Atmosphere Explorers C and E; DE-2 = Dynamics Explorer 2; GOCE = Gravity field and steady-state Ocean Circulation Explorer.

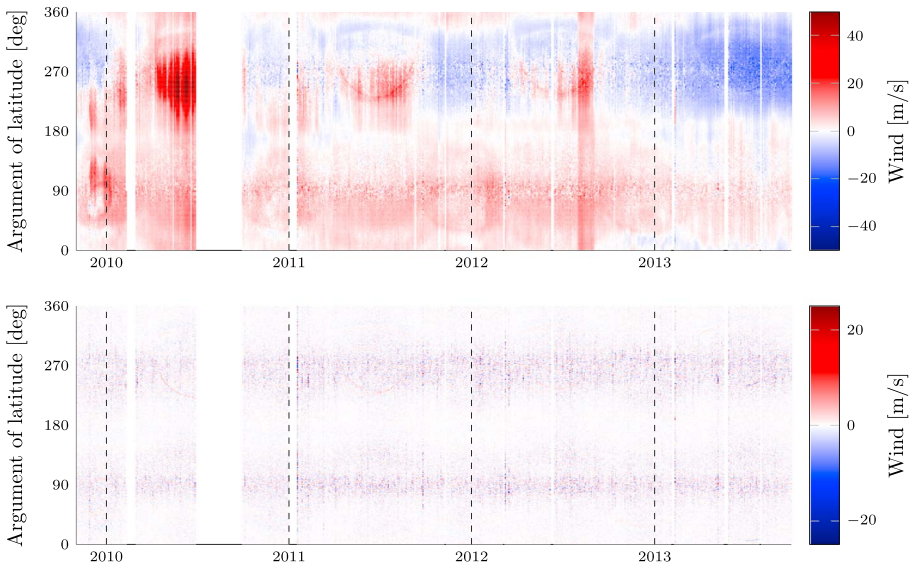

Figure 4. Vertical (upward) wind versus time and argument of latitude for the full GOCE mission (top panel) and the same data after high-pass filtering at 1/240 Hz (bottom). Note that the color scales are different in each panel.

that paper such that the mean vertical wind was zero. Without such estimates, the (stable) bias in the mean wind exceeded 100 m/s. Even after parameter estimation, a systematic offset of 30–40 m/s exists between the Northern and Southern Hemispheres. At the same time, the random error in the wind is expected to be much smaller, in the order of 3 m/s (3σ). Additionally, the uncertainty in the energy accommodation coefficient may cause a scale factor error up to 20% (if the coefficient in the aerodynamic model would be lowered to 0.60, see Visser et al., 2019, for details).

The complete GOCE vertical wind data set is plotted in Figure 4 against time and argument of latitude (i.e., the angular progress through the orbit, starting from the Northward equator crossing). The main large-scale feature is the difference between the Northern (0–180° argument of latitude) and Southern Hemispheres. Due to uncertainties in force and especially torque models, this low-frequency signal cannot be validated internally (Visser et al., 2019), and further research is required to find its cause. Due to the uncertainties in the vertical acceleration bias, it is unclear whether the mean wind is upward or downward. A second large-scale feature are the arcs between 200° and 270° argument of latitude, observed between April and September of each year. These arcs overlap with eclipse transitions (cf. Figure 7 of Visser et al., 2019) and are therefore attributed to an error in the transition model that was used to remove radiation pressure accelerations in the GOCE data processing. Similar arcs can be observed at different times and locations that do not align with eclipse transitions. The most important signal for the current discussion is the large amount of vertical wind peaks over the North (90°) and South Poles (270°). This signal is more clearly visible in the bottom panel of Figure 4, for which the data were filtered using a second-order high-pass Butterworth filter with a cutoff frequency of 1/240 Hz. The magnitude of these peaks exceeds 150 m/s on roughly 240 separate occasions spread out over the four 4-year mission.

3. Methodology

In order to compare our results directly with the related work of Innis and Conde (2002), we calculate their $\sigma(V_z)$ parameter for all satellite data sets. This is the standard deviation (σ) of the vertical wind (V_z) over a moving 120-s central window. This time interval corresponds to spatial scales of approximately 900–1,000 km. The window is moved by one data point at a time, to obtain a $\sigma(V_z)$ value for each data point in the original set. Both the vertical wind and $\sigma(V_z)$ are plotted for five representative passes in Figure 5. From visual inspection of the GOCE data, we conclude that vertical wind peaks span 30–90 s, and most vertical wind activity takes the form of wavelets of several consecutive upward and downward peaks. This implies that high $\sigma(V_z)$ values typically span one upward and one downward extremity. Signals that are significantly larger scale than the window (e.g., an offset due to the vertical acceleration bias uncertainty) will be filtered

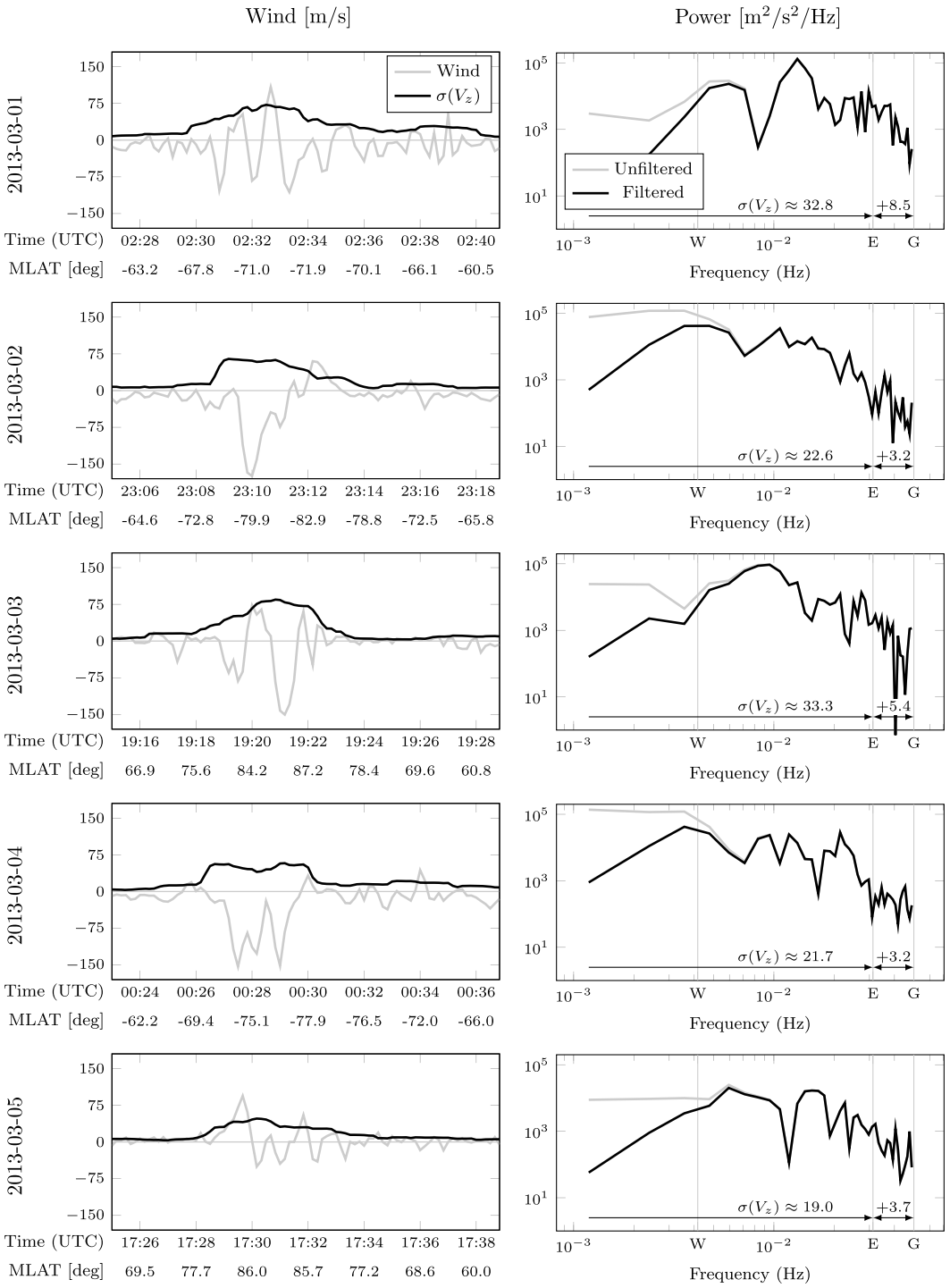

Figure 5. Time series (left) and periodograms (right) of vertical wind over the 14 min surrounding the largest peak of each of the first 5 days of March 2013. In the power spectra, the half-wave per $\sigma(V_z)$ window (1/240 Hz) and the Nyquist frequencies of the Explorer data (1/32 Hz) and the GOCE data (1/20 Hz) are indicated by the letters W, E, and G, respectively. Based on the periodograms, an estimate is made of the average $\sigma(V_z)$ value and the underestimation of this parameter due to the difference in data rate between the missions. MLAT = magnetic latitude.

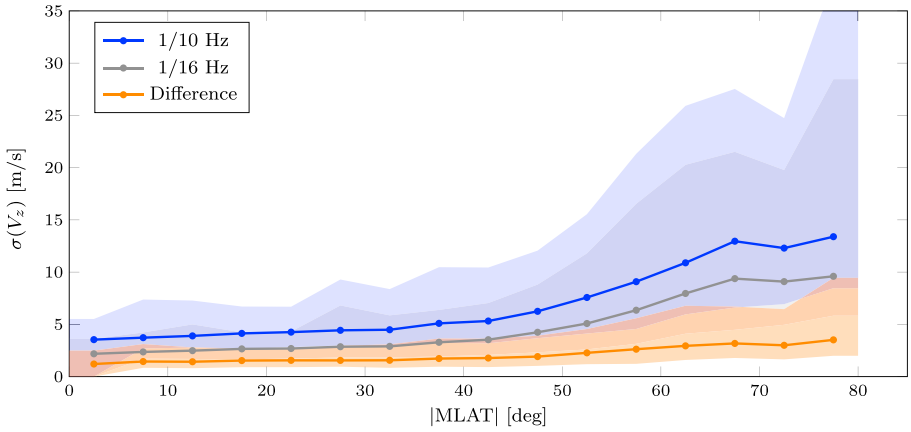

Figure 6. The average $\sigma(V_z)$ parameter over 15-min periods in March 2013, obtained for a data rate of 1/10 Hz, 1/16 Hz, and the difference between the two, in terms of the 5th, 50th, and 95th percentiles in 5° MLAT bins. MLAT = magnetic latitude.

out automatically by the calculation of the standard deviation, so we do not high-pass filter the original data set first.

The standard deviation of the data in a window is a measure for the total power represented by that data. If the temporal resolution of the data is higher, higher frequencies are represented, and the total power will increase. Within the current discussion, this will lead to an underestimation of $\sigma(V_z)$ for the Explorer missions as compared to GOCE. Therefore, we first note that while the GOCE accelerations are measured instantaneously (and the temporal resolution is therefore commensurate to the data rate), the baffle on the mass spectrometer takes about 2 s to perform a single sweep of ±24° (Spencer et al., 1973). The worst case temporal resolution is therefore 18 s. At 8 km/s orbital speed, however, a vertical wind of 150 m/s corresponds to an incidence angle of only 1°. Therefore, we expect that the peak wind has generally been measured close to the middle of the sweep, and we assume the temporal resolution did not deviate much from the data rate. The underestimation of $\sigma(V_z)$ can now be approximated for each pass in Figure 5 by integrating the periodogram between the Nyquist frequencies of the Explorer and GOCE data sets. Before integration, the periodograms are high-pass filtered using a second-order Butterworth filter with a cutoff frequency of 1/240 Hz, to simulate the effect of the moving 120-s window. The average $\sigma(V_z)$ and its expected underestimation by the Explorers are indicated for each pass in the periodograms in Figure 5. The same procedure was repeated for all consecutive 15-min time frames in March 2013. The results of this analysis are plotted against the mean magnetic latitude within the 15-min frame in Figure 6, in terms of the 5th and 95th percentile and the median in each bin. From Figures 5 and 6, we conclude that underestimation of $\sigma(V_z)$ by the Explorer missions is of the order of 1–2 m/s in the equatorial latitudes (where $\sigma(V_Z)$ is low) and increases with $\sigma(V_z)$ toward higher latitudes. In particularly disturbed times, such as the pass on 1 March 2013 shown in Figure 5, the underestimation may surpass 20% of the value found for GOCE.

The second source of discrepancy between $\sigma(V_z)$ data from GOCE and the Explorer missions is the difference in noise level. Since $\sigma(V_z)$ reflects the total power in the measurements, it should ideally be corrected for the noise power (Chu et al., 2018). The noise in the GOCE accelerometer data causes a vertical wind standard deviation below 1 m/s (see Table 4 of Visser et al., 2019) and is therefore ignored here. For the Explorer missions only, the total error of the measurements is known, and the noise level can therefore not be corrected for.

Because of its definition as the standard deviation of the (centrally distributed) vertical wind, $\sigma(V_z)$ is approximately Gamma-distributed. We find that the difference between data sets can be approximated by a single-scale factor, defined as the ratio between the means. Assuming the vertical wind is zero mean, the scale factor of the standard deviation would directly apply to the vertical wind itself. This allows us to check whether the difference between accelerometer and mass spectrometer data can be explained by a single-scale factor, such as is caused by a different choice of accommodation coefficient within the GOCE wind processing (Visser et al., 2019).

The different data sets are compared in terms of their probability densities. These values are calculated by binning the data over 0.5 or 1 m/s bins and subsequently dividing the amount of data in each bin by the total amount of data points and the bin width. To evaluate the uncertainty of the density in each bin, a Monte Carlo method is applied. In this method, the process of calculating the probability density is repeated for subsets of the data. These subsets are selected by dividing the $\sigma(V_z)$ time series into consecutive 120-s sections. From each section, the first data point is selected (out of 12 for GOCE and 7 for the Explorer missions) to find the first probability density, then the second data point is selected to find the second distribution, and so on. This process results in 12 probability densities for GOCE or 7 for the Explorer missions. The maximum and minimum densities in each bin from this set of distributions are used as the uncertainty bounds. The same approach is used to find the uncertainty in the ratio between the means. In that case, however, the maximum uncertainty is found by dividing the maximum and minimum means of one data set by the minimum and maximum of the other data set, respectively. The largest deviation from the original ratio is used as the uncertainty.

Before comparing the different missions, we identify the driving parameters. From the literature and the GOCE data, we can identify four such parameters: magnetic latitude, magnetic local time, season, and geomagnetic activity. To quantify the last, we use the hourly Auroral Electrojet (AE) index by default. As the AE index is not available for the years 1976–1977, we use the Kp index when we compare GOCE to the Atmosphere Explorers. In line with Innis and Conde (2002), we impose a maximum measurement altitude of 450 km.

In each comparison, we select a specific range of all the above parameters. First and foremost, the magnetic latitude range is split in the low latitude (0–30°), midlatitude (30–60°), auroral latitude (60–80°), and polar cap latitude (80–90°) ranges. Magnetic local time is either set manually or selected automatically based on the GOCE orbit. In this process the magnetic local time is split in 48 half-hour bins, in which the lowest Northern and Southern magnetic latitudes are found for which GOCE data are available. After distributing all satellite data over the mesh of magnetic local time, only those data are kept that lie within these magnetic latitude bounds in each bin. We will refer to the remaining data as being a member of the GOCE orbit geometry. To account for seasonal variations, we divide the year in four periods: December solstice (November–January), March equinox (February–April), June solstice (May–July), and September equinox (August–October). When studying seasonal variations, the Northern and Southern Hemispheres are treated separately. Finally, we use the bounds on the AE index that were selected by Innis and Conde (2002), being low ($AE \leq 250$), medium ($250 < AE \leq 500$), and high ($AE > 500$) activities.

After validating the GOCE vertical wind activity data, we investigate the impact of certain parameters on the vertical wind activity in terms of $\sigma(V_z)$. First, we distribute the data over preset bins of a parameter of interest. Then in each bin, the 5th, 25th, 50th, 75th, and 95th percentiles of $\sigma(V_z)$ are calculated and plotted. The number of data points in each bin serves to quantify the confidence level of the percentiles in that bin. To allow for a high resolution in the driving parameter, no further constraints are placed on other driving parameters, unless stated otherwise.

4. Validation

The force-derived vertical wind data set described in this paper is extensively compared to torque-derived data by Visser et al. (2019). The latter are dominated by the effects of model errors, but a high-pass filtered version is shown to be consistent with the force-derived wind within 50 m/s. In this section, we compare the $\sigma(V_z)$ data derived from forces acting on GOCE to those obtained from the other satellite missions listed in Table 1.

In Figure 7, the GOCE data are compared to the DE-2 data by plotting the probability density distributions of the $\sigma(V_z)$ data in the auroral and polar cap regions, over three levels of geomagnetic activity. For all plots, only data are used that lie in the GOCE orbit geometry (as defined in section 3) and at altitudes below 450 km. Seasonal effects are ignored, as they are insignificant (less than 5 m/s $\sigma(V_z)$) at these high latitudes, and both GOCE and DE-2 provide uniform coverage of the seasons (see Figure 3).

Especially at the polar cap, the similarity between the two data sets over the full range of geomagnetic activity is striking. This is confirmed by the ratio of the means, included in the legend of each plot, which does not exceed 5%. In the auroral region, the differences are larger, starting from 21% at low geomagnetic activity

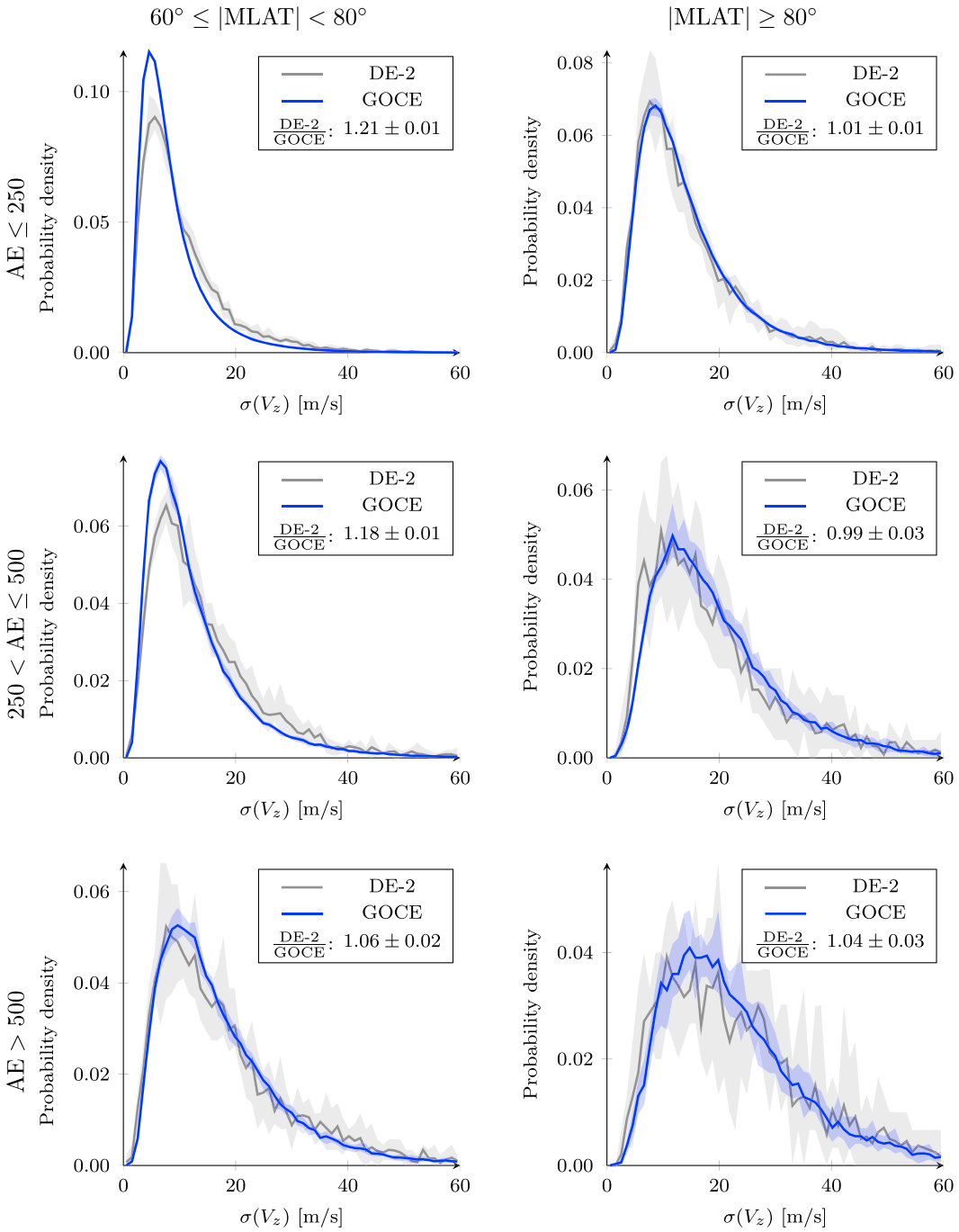

Figure 7. Probability density of the $\sigma(V_z)$ data of GOCE, compared to that of DE-2, in the auroral (left) and polar cap latitudes (right), for different levels of geomagnetic activity. DE-2 = Dynamics Explorer 2; GOCE = Gravity field and steady-state Ocean Circulation Explorer; AE =Auroral Electrojet; MLAT = magnetic latitude.

levels, decreasing to 6% at high activity. From the spectral analysis, however, an underestimation of $\sigma(V_z)$ by DE-2 was expected. This discrepancy may be explained by the higher random error in the DE-2 data or by a too low accommodation coefficient in the aerodynamic model of the GOCE satellite. Previous results have however indicated that the latter parameter should rather be reduced than increased to improve the consistency of the GOCE wind data (Visser et al., 2019).

Performing the same analysis at low and middle latitudes, we can include data from AE-E and AE-C, respectively (see Figure 8). At (magnetic) latitudes below 60°, seasonal effects play an important role, whereas the

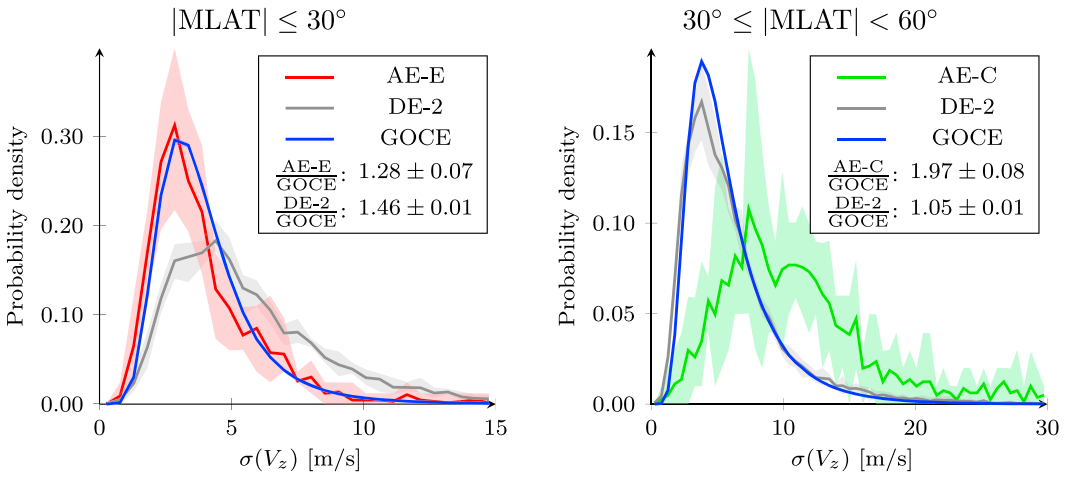

Figure 8. Probability density of the $\sigma(V_z)$ data of GOCE, compared to that of DE-2 and the available Atmosphere Explorer, in the equatorial (left) and middle latitudes (right), both using only the June and December solstice months and adhering to the GOCE orbit geometry. AE-C and AE-E = Atmosphere Explorers C and E; DE-2 = Dynamics Explorer 2; GOCE = Gravity field and steady-state Ocean Circulation Explorer; MLAT = magnetic latitude.

effect of geomagnetic storms dies out. Therefore, we limit our comparison to the solstice months, in which all AE-E and most of the AE-C data were gathered. At the same time, a wide range of Kp values is included, selecting all Kp levels for which data from all plotted satellites are available. As before, the comparison is limited to the GOCE orbit geometry and altitudes below 450 km. Although all AE-E data lie below 20° latitude, the magnetic latitude regularly peaks at 30°, allowing us to use this limit in this comparison.

In the low-latitude region, the GOCE data align very well with the AE-E data, while the DE-2 distribution is drawn to higher vertical wind levels. We do note however that the peaks of the distributions lie at or below the maximum expected random error for all satellites and may therefore be significantly impacted by the power of the measurement noise. This complicates the validation of the GOCE data in this latitude range. On top of that, the amount of data that is left from the mass spectrometer missions is limited. For AE-E only, 1,295 data points remain after data selection. This may explain the high ratio of means between this satellite and GOCE, despite the visual resemblance between the lines.

In the midlatitude range, GOCE lines up with DE-2, as was the case at higher latitudes. The consistency with the AE-C data is rather poor, with significantly higher vertical wind activity. As was the case for AE-E, only a small amount of AE-C data (1,640 points) remains after the selection procedure. Consequently, a small amount of anomalous passes may bias the overall result, as is reflected by the wide and erratic uncertainty bounds.

Despite the discrepancies between the different satellites at low and middle latitudes, which still require an explanation, we observe that GOCE always lines up well with one of the other satellites. This is an important result, as it suggests that there is no inherent bias between the different measurement techniques.

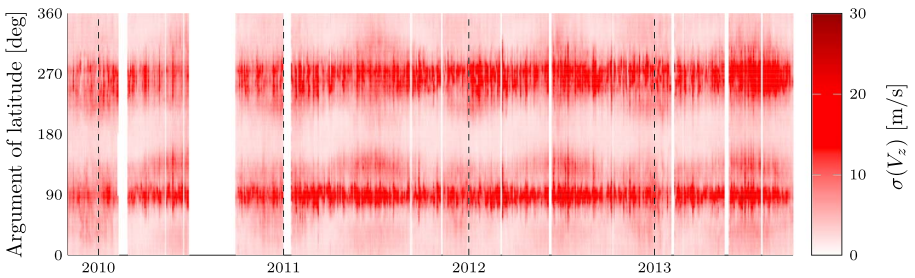

Figure 9. Moving-window standard deviation of vertical wind $\sigma(V_z)$ versus time and argument of latitude for the full GOCE mission.

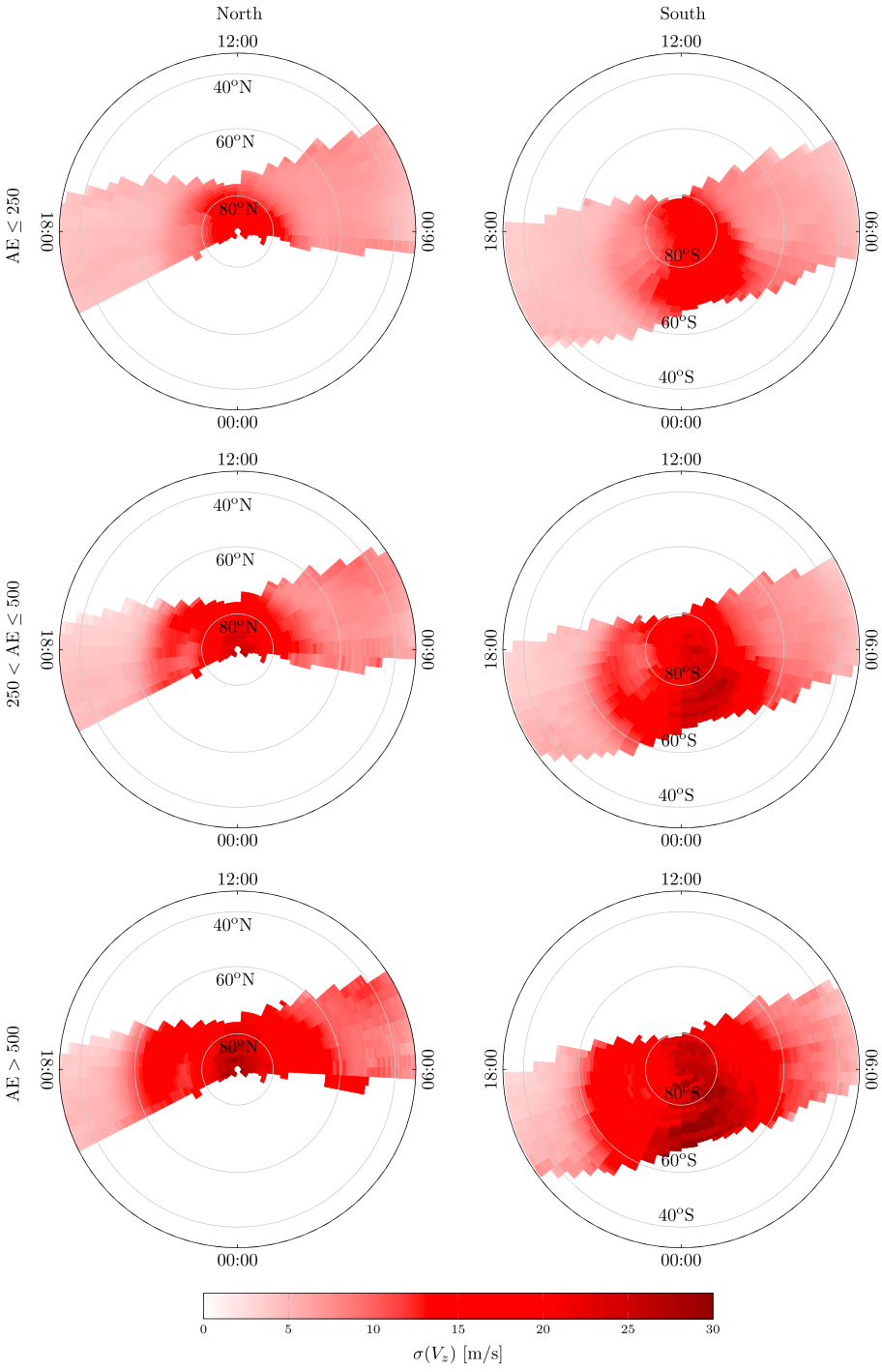

Figure 10. Standard deviation $\sigma(V_z)$ versus magnetic latitude and magnetic local time over the North (left) and South Pole (right) for different levels of geomagnetic activity in terms of AE. AE = Auroral Electrojet.

5. Results

The main feature of interest in vertical wind data is the collection of large extrema in the auroral zone and over the polar caps (around 90° and 270° argument of latitude). This is best illustrated by the $\sigma(V_z)$ parameter, plotted in Figure 9 for the full mission. The highest activity is concentrated at high latitudes. Especially during local summer, this area expands toward the descending node (180°), which corresponds to the dawn sector of the orbit.

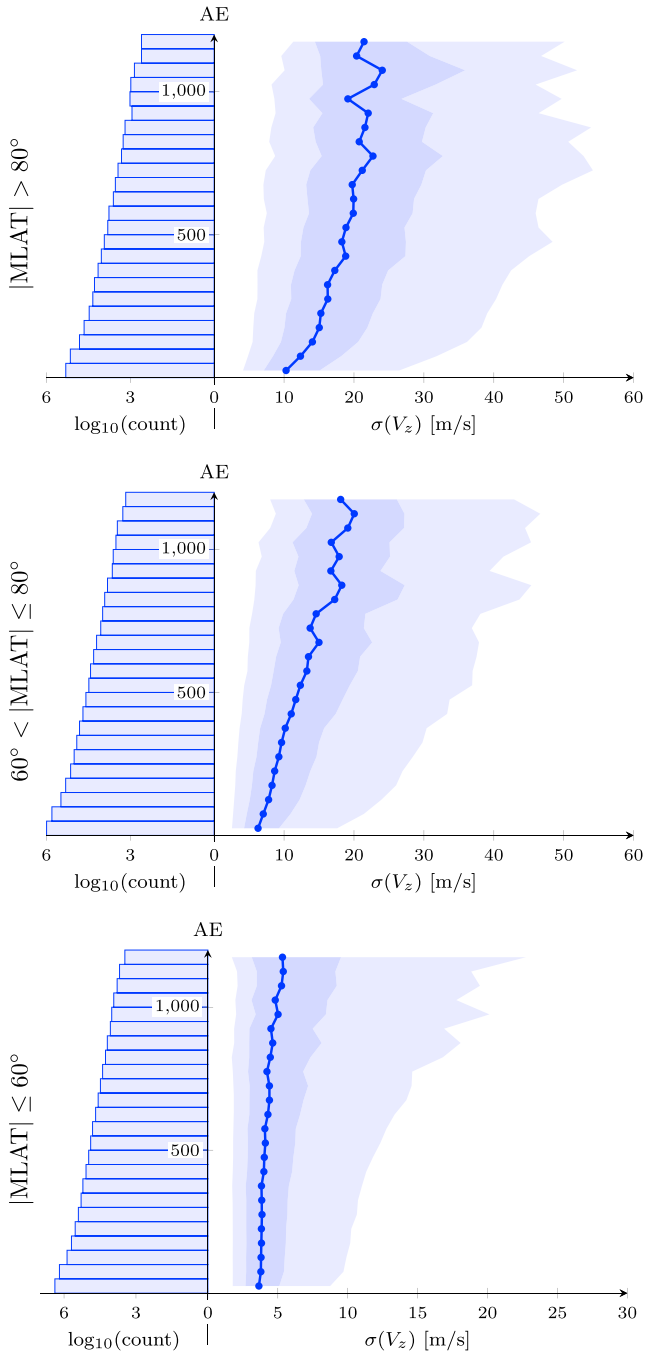

Figure 11. Percentiles (5th, 25th, 50th, 75th, and 95th) of $\sigma(V_z)$ and data count, per bin of AE index, over the polar cap (top), auroral oval (middle), and low and middle latitudes (bottom). MLAT = magnetic latitude; AE = Auroral Electrojet.

The extra vertical wind activity in the midnight-dawn sector and its response to increased geomagnetic activity reported by Innis and Conde (2002) is confirmed for the South Pole by the data obtained from GOCE. This is illustrated by the polar plots in Figure 10, which correspond directly to Figures 6–8 of Innis and Conde (2002). Note that this specific local time sector is out of GOCE's view over the North Pole.

The size of the new GOCE data set allows us to look at the effect of different parameters on the vertical wind activity in the different latitude ranges in great detail. Because apart from the magnitude, no significant difference was found between the vertical wind in the low and middle latitude regimes, those regions are

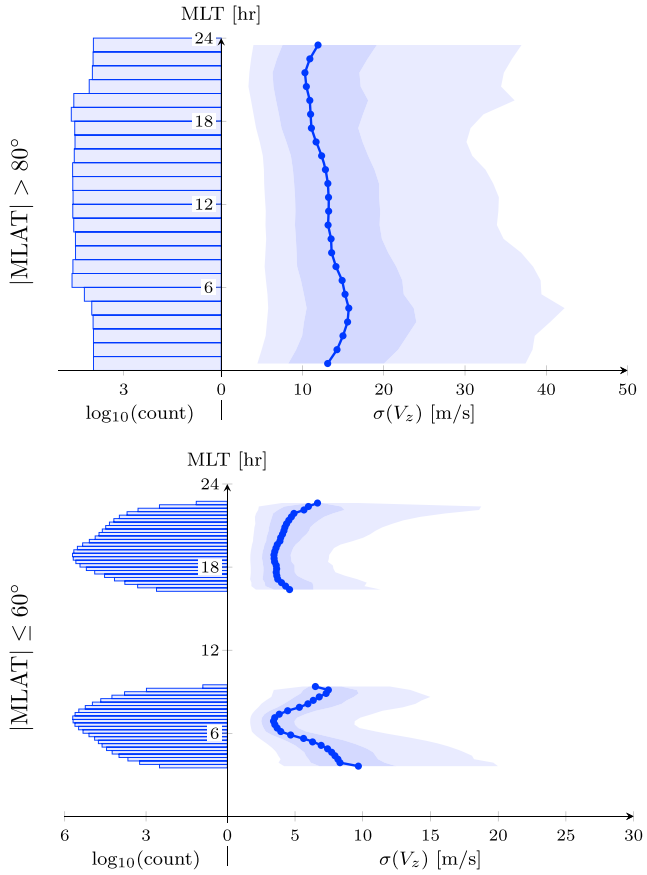

Figure 12. Percentiles (5th, 25th, 50th, 75th, and 95th) of $\sigma(V_z)$ and data count, per bin of MLT, over the polar cap (top, bin width 1 hr) and low and middle latitudes (bottom, bin width 15 min). MLAT = magnetic latitude; MLT = magnetic local time.

combined for the remainder of this discussion. The result of the statistical analysis is presented in plots like Figure 11. Here the light-shaded area is bounded by the 5th and 95th percentiles, the darker-shaded area indicates the first and third quartiles, and the marked line connects the medians. The histogram to the left indicates the amount of data points in each bin. A large peak in $\sigma(V_z)$ can maintain a level above 80 m/s for several minutes, resulting in 20–40 data points at 0.1 Hz. In our experience, this means that bins containing less than 1,000 data points are particularly sensitive to outlier events.

The first parameter that we discuss in more detail is the AE index for geomagnetic activity. In Figure 11, the percentiles are plotted for the three magnetic latitude ranges. Over the polar cap, the vertical wind response to geomagnetic activity seems to level out for AE values above 800, at $\sigma(V_z)$ levels of 10–50 m/s (in terms of the 5th and 95th percentiles). A similar trend can be observed in the auroral region at the highest percentile. The fact that the other percentiles follow a linear increasing trend may be explained by the limited latitude extent of the auroral oval within the selected latitude range. Only part of the latitude range is covered by the area of increased $\sigma(V_z)$, and this part increases with increasing geomagnetic activity. The increasing trend in $\sigma(V_z)$ at high AE values in the low and middle latitudes is caused by the auroral oval moving down into the midlatitude region.

The geomagnetic response observed as a function of the AE index does not depend on the choice of index. No important difference has been observed when using the (equatorial) Dst, Polar Cap, or Kp index. The benefit of AE over Kp is that the former is linear and continuous, improving the resolution in the high activity domain of Figure 11.

The second parameter of interest is magnetic local time. Although its influence on the vertical wind was analyzed in the context of the polar plots in Figure 10, the percentiles in Figure 12 provide a higher resolution, as well as a view of the low to middle latitudes. Over the polar cap, the distribution of vertical wind

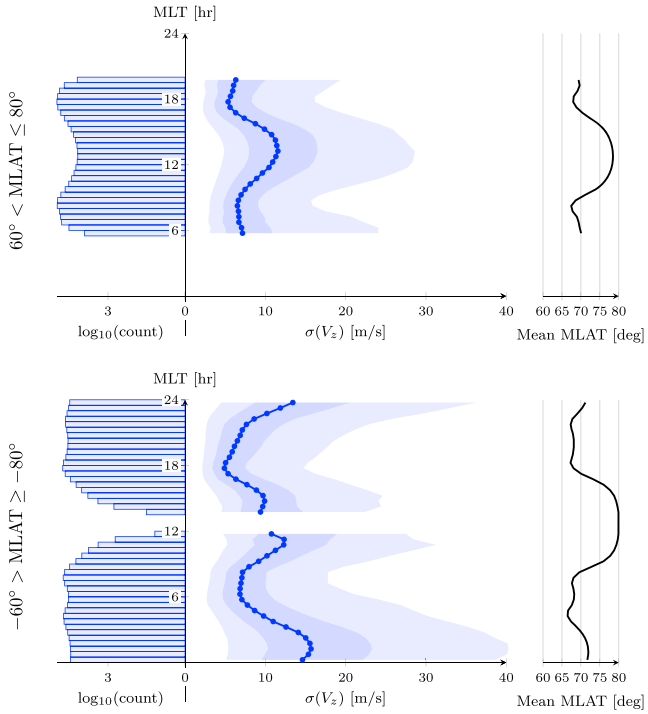

Figure 13. Percentiles (5th, 25th, 50th, 75th, and 95th) of $\sigma(V_z)$ and data count, per bin of MLT, over the Northern (top, bin width 30 min) and Southern auroral oval (bottom, bin width 30 min). MLAT = magnetic latitude; MLT = magnetic local time.

over local time is most uniform, with a peak around 04:30 and a dip around 21:00. In the auroral region, plotted separately for the two hemispheres in Figure 13, the distribution is much more pronounced. Clear peaks are observed at 01:15 (Southern Hemisphere) and 13:15 (Northern Hemisphere) and dips between 06:00 and 08:30 and at 17:45. Although especially the peaks can also be observed in Figure 10, the location of these extremities is predominantly driven by the nonuniform coverage of magnetic latitude at different local times. This is illustrated by the mean magnetic latitude in each bin, plotted on the right of Figure 13. A close correlation is observed between the location of the $\sigma(V_z)$ extremities and the mean magnetic latitude in each bin. At the low and middle latitudes (in Figure 12), the peaks are lost due to the orbit geometry, but the dips remain visible at 06:45 and 19:00.

Third, we observe seasonal effects in the vertical wind, especially in the low to middle latitudes. This is illustrated in Figures 14 and 15 for the Northern and Southern Hemispheres, respectively. In the low to middle latitudes, the vertical wind activity dips in the equinox months and peaks in both the June and December solstice months. The trend shows resemblance, if an inverted one, to the semiannual density variation. It is unlikely that the change in thermospheric composition will cause a large enough variation in the aerodynamic model to explain the entire difference between equinox and solstice (see Table 5 of ; Visser et al., 2019, and Figure 3.9 of ; Doornbos, 2011). It is possible that the mechanism driving the semiannual density variation (e.g. the "thermospheric spoon" suggested by ; Fuller-Rowell, 1998) also increases the vertical wind activity. A significant influence of the orbit geometry is unlikely, as the distribution over magnetic local time is mostly constant throughout the year (see Figure 3). At the polar cap, the seasonal trends are more erratic, but the peak winds seem to be concentrated around the local summer solstice. Although this observation would contradict the reduction in wind activity with increased solar illumination observed by Innis and Conde (2002), it does confirm their conclusion that the effect is marginal. The trend in the auroral region seems to reflect a gradual transition from the low to the high latitudes.

Finally, we note that the vertical wind response to the observed F10.7 flux is similar for all latitude ranges and weak overall. This is shown in Figure 16, where only the 95th percentile increases slightly, although not very consistently, with increasing solar flux. This increase may be explained by an overall increase in geomagnetic activity with increasing solar activity, rather than a direct solar radiation effect.

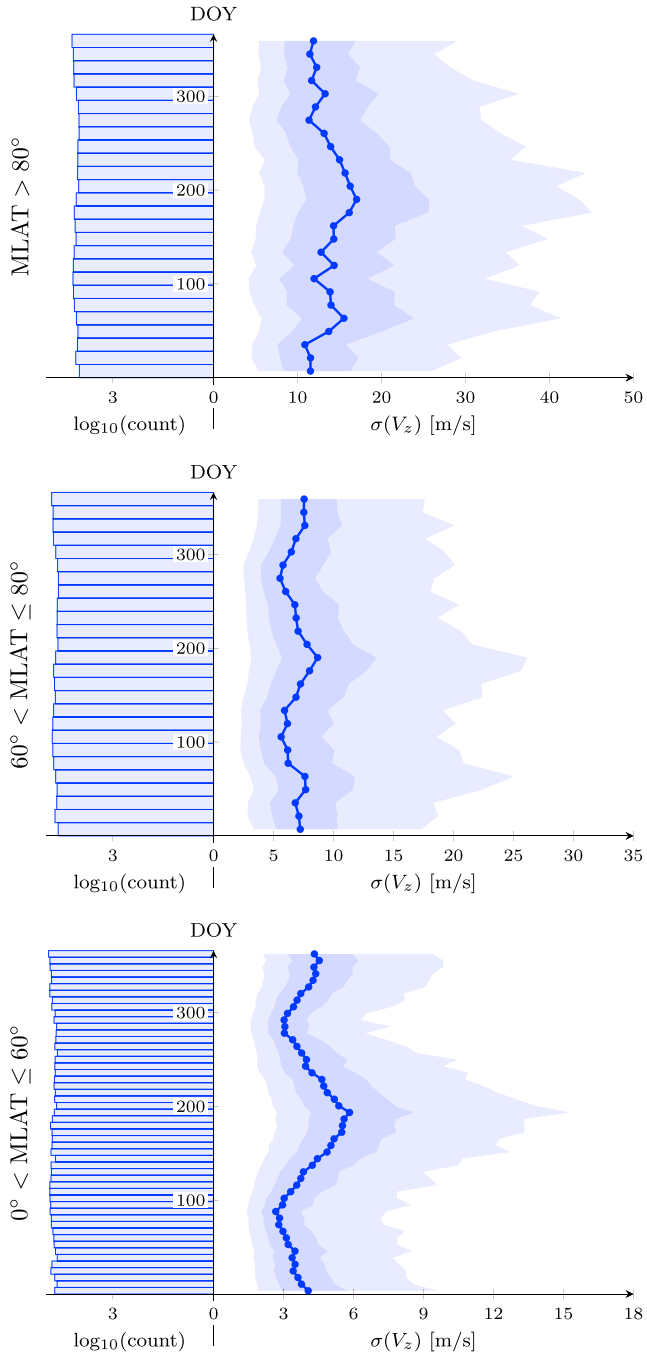

Figure 14. Percentiles (5th, 25th, 50th, 75th, and 95th) of $\sigma(V_z)$ and data count, per bin of DOY, over the Northern polar cap (top, bin width 2 weeks), auroral oval (middle, bin width 2 weeks), and low and middle latitudes (bottom, bin width 1 week). MLAT = magnetic latitude; DOY = day of year.

6. Conclusion

Despite the different sampling rate and uncertainty characteristics of the GOCE accelerometer data compared to the mass spectrometer data of AE-C, AE-E, and DE-2, we conclude that the vertical accelerations of the GOCE satellite are a valid source of vertical wind activity data. From the comparison, in terms of the moving-window standard deviation $\sigma(V_z)$, with the data of the DE-2 satellite at middle and high latitudes, no structural error was found in the accelerometer-derived vertical wind. In the midlatitude range, the AE-C winds disagree with the other two satellites. Given the scarcity of these data, outlier events may have had a

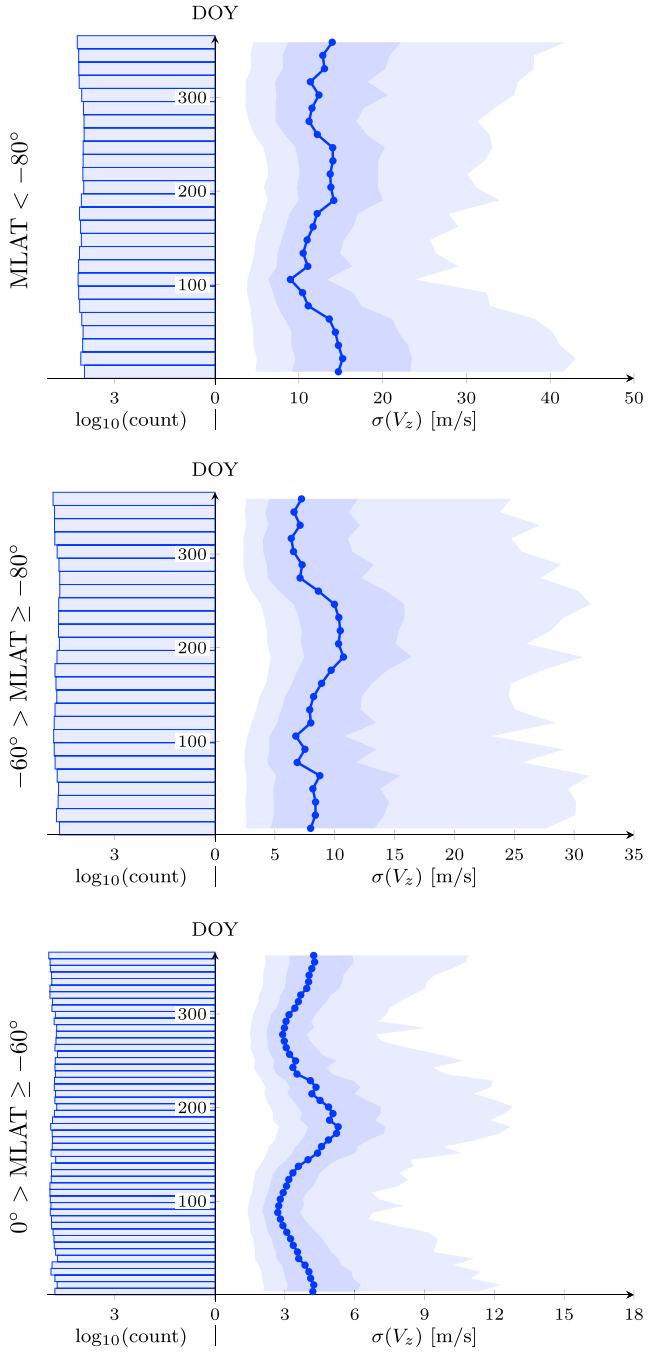

Figure 15. Percentiles (5th, 25th, 50th, 75th, and 95th) of $\sigma(V_z)$ and data count, per bin of DOY, over the Southern polar cap (top, bin width 2 weeks), auroral oval (middle, bin width 2 weeks), and low and middle latitudes (bottom, bin width 1 week). MLAT = magnetic latitude; DOY = day of year.

significant influence on this discrepancy. In the low-latitude regime, the $\sigma(V_z)$ probability distributions peak close to the expected maximum random error level of the respective data sets. Nevertheless, a close match is found between the GOCE and AE-E data.

The result of this process is a vertical wind data set, validated for short time scales of at least 120 s, that single-handedly increases the amount of available measurements from satellites with a factor of 27. In total, 1,100 full days of data containing 16 orbits each and an additional 170 partial days are available, spread out over 4 years. Due to the orbit geometry, near global coverage is provided at an altitude between 230 and 290

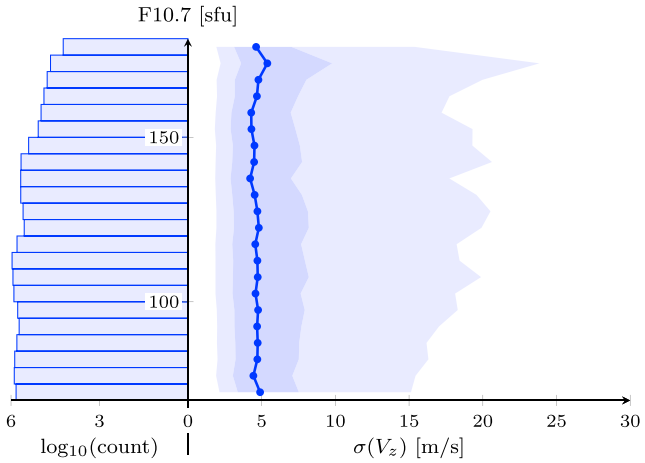

Figure 16. Percentiles (5th, 25th, 50th, 75th, and 95th) of $\sigma(V_z)$ and data count, per bin of F10.7 flux, over the full latitude range.

km, limited in local time to dawn and dusk conditions. Data are available for low to medium solar activity and a wide range of geomagnetic activity levels.

The size of the data set allowed for a high-resolution investigation into the driving parameters of the vertical wind activity. Most importantly, a maximum vertical wind activity is observed in the response of the thermosphere to increased geomagnetic activity. In terms of the $\sigma(V_z)$ parameter, the 95th percentile is expected to level out around 50 m/s activity levels, for AE index values above 800. In other geomagnetic indices, the same behavior was observed.

Over the polar cap, a single peak in activity is observed in the midnight-dawn sector, but the overall response is mostly uniform over the magnetic local time range. In the auroral latitude range, the structure in local time is much more pronounced but predominantly driven by the nonuniform coverage of magnetic latitude at different local times. At equatorial latitudes, dips were observed around 06:00 and 18:00 magnetic local time.

Seasonal variations are much smaller than the above effects but are the dominant driver in the lower latitudes at fixed local times. Both on the Northern and Southern Hemispheres, the peak activity occurs around June solstice, with the December solstice producing a smaller peak. This seasonal variation resembles the semiannual density variation, which is thought to be caused by increased interhemispheric circulation at the solstices. At the polar cap, indications were found for a single peak just after local summer solstice, but more research is required to confirm this observation. Solar activity, in terms of the observed solar flux, does not influence the vertical wind activity.

Although the results of this paper are promising, we do not expect a new accelerometer-derived vertical wind data set to be produced soon. The GOCE mission was unique in both its low altitude and its exceptionally sensitive accelerometers , but also the availability of high quality housekeeping data, like the thrust level. This combination led to an especially high aerodynamic signal and the ability to actually detect and interpret it. It is however worth investigating whether similar observations can be made using other existing accelerometer-carrying satellites, such as GRACE and CHAMP, or future mission concepts, such as the proposed ESA Earth Explorer 10 candidate mission Daedalus (Sarris et al., 2019).

Data Statement

The GOCE thermospheric data used in this study are publicly available at http://eo-virtual-archive1.esa.int/GOCE-Thermosphere.html after requesting access online (https://earth.esa.int/web/guest/-/goce-data-access-7219). The Atmosphere Explorer and Dynamics Explorer data are publicly available through NASA's OmniWeb service (https://omniweb.gsfc.nasa.gov/ftpbrowser/index.html). The AE index library is maintained by Kyoto University and publicly available online (http://wdc.kugi.kyoto-u.ac.jp/dstae/index.html). The observed F10.7 flux is available on the NOAA ftp server (ftp://ftp.ngdc.noaa.gov/STP/space-weather/solar-data/solar-features/solar-radio/noontime-flux/penticton/penticton_observed/tables/).

Acknowledgments
The European Space Agency (ESA) is acknowledged for supporting this study in the framework of the GOCE High Level Processing Facility (HPF). The authors would like to thank ESA, specifically Micheal Fehringer, Björn Fromknecht, and Rune Floberghagen, for their support in accessing the GOCE data and documentation, NASA for providing their OmniWeb service, and Kyoto University for maintaining the AE index. The polar plots in Figure 10 were generated in Matlab using the `M_Map` package and then converted to pdf format using `matlab2tikz`.

References

Anderson, C., Conde, M., & McHarg, M. G. (2012). Neutral thermospheric dynamics observed with two scanning Doppler imagers: 2. Vertical winds. *Journal of Geophysical Research*, *117*, A03305. https://doi.org/10.1029/2011JA017157

Aruliah, A. L., & Rees, D. (1995). The trouble with thermospheric vertical winds: Geomagnetic, seasonal and solar cycle dependence at high latitudes. *Journal of Atmopsheric and Terrestrial Physics*, *57*(6), 597–609. https://doi.org/10.1016/0021-9169(94)00100-3

Chu, X., Zhao, J., Lu, X., Harvey, V., Jones, R., Becker, E., et al. (2018). Lidar observations of stratospheric gravity waves from 2011 to 2015 at McMurdo (77.84°S, 166.69°E), Antarctica: 2. Potential energy densities, lognormal distributions, and seasonal variations. *Journal of Geophysical Research: Atmospheres*, *123*, 7910–7934. https://doi.org/10.1029/2017JD027386

Doornbos, E. N. (2011). *Thermospheric density and wind determination from satellite dynamics*. Berlin, Heidelberg, Germany: Springer. https://doi.org/10.1007/978-3-642-25129-0

Doornbos, E. N. (2016). GOCE+ Theme 3: Air density and wind retrieval using GOCE data: Data set user manual. ESA AO/1-6367/10/NL/AF.

Floberghagen, R., Fehringer, M., Lamarre, D., Muzi, D., Frommknecht, B., Steiger, C., et al. (2011). Mission design, operation and exploitation of the Gravity field and steady-state Ocean Circulation Explorer mission. *Journal of Geodesy*, *85*(11), 749–758. https://doi.org/10.1007/s00190-011-0498-3

Fuller-Rowell, T. (1998). The "thermospheric spoon": A mechanism for the semiannual density variation. *Journal of Geophysical Research*, *103*(A3), 3951–3956. https://doi.org/10.1029/97JA03335

Garcia, R. F., Bruinsma, S., Lognonné, P., Doornbos, E., & Cachoux, F. (2013). GOCE: The first seismometer in orbit around the Earth. *Geophysical Research Letters*, *40*, 1015–1020. https://doi.org/10.1002/grl.50205

Harding, B. J., Makela, J. J., Qin, J., Fisher, D. J., Martinis, C. R., Noto, J., & Wrasse, C. M. (2017). Atmospheric scattering effects on ground-based measurements of thermospheric vertical wind, horizontal wind, and temperature. *Journal of Geophysical Research: Space Physics*, *122*, 7654–7669. https://doi.org/10.1002/2017JA023942

Hoffman, R. A. (1980). Dynamics Explorer Program. *Eos, Transactions American Geophysical Union*, *61*(44), 689–692. https://doi.org/10.1029/EO061i044p00689

Innis, J. L., & Conde, M. (2002). High-latitude thermospheric vertical wind activity from Dynamics Explorer 2 Wind and Temperature Spectrometer observations: Indications of a source region for polar cap gravity waves. *Journal of Geophysical Research*, *107*(A8), 1172. https://doi.org/10.1029/2001JA009130

Innis, J. L., Greet, P. A., Murphy, D. J., Conde, M. G., & Dyson, P. L. (1999). A large vertical wind in the thermosphere at the auroral oval/polar cap boundary seen simultaneously from Mawson and Davis, Antarctica. *Journal of Atmospheric and Solar-Terrestrial Physics*, *61*, 1047–1058. https://doi.org/10.1016/S1364-6826(99)00060-7

Knutson, J. R., Kayser, D. C., & Potter, W. E. (1977). Mass spectrometric measurements of thermospheric wind. *Journal of Geophysical Research*, *82*(32), 5253–5256. https://doi.org/10.1029/JA082i032p05253

Larsen, M. F., & Meriwether, J. W. (2012). Vertical winds in the thermosphere. *Journal of Geophysical Research*, *117*, A09319. https://doi.org/10.1029/2012JA017843

Neil Davis, Thomas, & Sugiura, Masahisa (1966). Auroral electrojet activity index AE and its universal time variations. *Journal of Geophysical Research*, *71*(3), 785–801. https://doi.org/10.1029/JZ071i003p00785

Sarris, T., Talaat, E., Palmroth, M., Dandouras, I., Armandillo, E., Kervalishvili, G., et al. (2019). Daedalus: A low-flying spacecraft for the exploration of the lower thermosphere-ionosphere. Geoscientific Instrumentation, Methods and Data Systems, under review, https://doi.org/10.5194/gi-2019-3

Sipler, D. P., Biondi, M. A., & Zipf, M. E. (1995). Vertical winds in the midlatitude thermosphere from Fabry–Perot Interferometry measurements. *Journal of Atmospheric and Terrestrial Physics*, *57*(6), 621–629. https://doi.org/10.1016/0021-9169(94)00102-T

Smith, R. W., & Hernandez, G. (1995). Vertical winds in the thermosphere within the polar cap. *Journal of Atmospheric and Terrestrial Physics*, *57*(6), 611–620. https://doi.org/10.1016/0021-9169(94)00101-S

Spencer, N. W., Brace, L. H., & Grimes, D. W. (1973). The Atmosphere Explorer spacecraft system. *Radio Science*, *8*(4), 267–269. https://doi.org/10.1029/RS008i004p00267

Spencer, N. W., Niemann, H. B., & Carignan, G. R. (1973). The neutral-atmosphere temperature instrument. *Radio Science*, *8*(4), 287–296. https://doi.org/10.1029/RS008i004p00287

Spencer, N. W., Theis, R. F., Wharton, L. E., & Carignan, G. R. (1976). Local vertical motions and kinetic temperature from AE-C as evidence for aurora-induced gravity waves. *Geophysical Research Letters*, *3*(6), 313–316. https://doi.org/10.1029/GL003i006p00313

Spencer, N. W., Wharton, L. E., Carignan, G. R., & Maurer, J. C. (1982). Thermosphere zonal winds, vertical motions and temperature as measured from Dynamics Explorer. *Geophysical Research Letters*, *9*(9), 953–956. https://doi.org/10.1029/GL009i009p00953

Trinh, Q. T., Ern, M., Doornbos, E., Preusse, P., & Riese, M. (2018). Satellite observations of middle atmosphere-thermosphere vertical coupling by gravity waves. *Annales Geophysicae*, *36*(2), 425–444. https://doi.org/10.5194/angeo-36-425-2018

Visser, T., March, G., Doornbos, E., de Visser, C., & Visser, P. (2019). Horizontal and vertical thermospheric cross-wind from GOCE linear and angular accelerations. *Advances in Space Research*, *63*(10), 3139–3153. https://doi.org/10.1016/j.asr.2019.01.030